Bioactive Materials 35 (2024) 330–345

Contents lists available at ScienceDirect

Bioactive Materials

journal homepage: www.keaipublishing.com/en/journals/bioactive-materials

Versatile dopamine-functionalized hyaluronic acid-recombinant human collagen hydrogel promoting diabetic wound healing via inflammation control and vascularization tissue regeneration

Yong Wang [a,1], Yuan Zhang [a,1], Yun-Peng Yang [a,1], Ming-Yuan Jin [a], Sha Huang [a], Ze-Ming Zhuang [a], Tao Zhang [a], Li-Li Cao [a], Xiao-Ying Lin [a], Jun Chen [a,d], Yong-Zhong Du [a,c], Jian Chen [b,**], Wei-Qiang Tan [a,*]

[a] Department of Plastic Surgery, Sir Run Run Shaw Hospital, Zhejiang University School of Medicine, 3 East Qingchun Road, Hangzhou, 310016, China
[b] Department of Ultrasound in Medicine, The Fourth Affiliated Hospital, Zhejiang University School of Medicine, Yiwu, 322000, China
[c] Institute of Pharmaceutics, College of Pharmaceutical Sciences, Zhejiang University, 866 Yu-Hang-Tang Road, Hangzhou, 310058, China
[d] MOE Key Laboratory of Biosystems Homeostasis & Protection, College of Life Sciences, Zhejiang University, Hangzhou, 310058, China

ARTICLE INFO

Keywords:
Hyaluronic acid hydrogel
Recombinant human collagen
Antioxidant and anti-inflammation
Antibacterial
Diabetic wound

ABSTRACT

The management of chronic wounds in diabetes remains challenging due to the complexity of impaired wound healing, delayed healing, susceptibility to infection, and elevated risk of reopening, highlighting the need for effective chronic wound management with innovative approaches such as multifunctional hydrogels. Here, we have produced HA-DA@rhCol hydrogels consisting of dopamine-modified hyaluronic acid and recombinant human collagen type-III (rhCol) by oxidative coupling of the catechol group using the H_2O_2/HRP catalytic system. The post-reactive hydrogel has a good porous structure, swelling rate, reasonable degradation, rheological and mechanical properties, and the catechol group and dopamine impart to the hydrogel tissue adhesiveness, antioxidant capacity, and excellent photothermal effects leading to superior in vitro antimicrobial activity. In addition, the ability of rhCol to confer hydrogels to promote angiogenesis and wound repair has also been investigated. Cytotoxicity and hemolysis tests demonstrated the good biocompatibility of the hydrogel. Wound closure, collagen deposition and immunohistochemical examination confirmed the ability of the hydrogel to promote diabetic wound healing. In summary, the adhesive hemostatic antioxidative hydrogel with rhCol to promote wound healing in diabetic rat is an excellent chronic wound dressing.

1. Introduction

The healing process of skin wounds is a complex cascade of events involving inflammation, cell proliferation, tissue formation, and remodeling [1,2]. In diabetic individuals, this process is disrupted, the accumulation of advanced glycation end products (AGEs) in the extracellular matrix contributes to tissue stiffness, limiting cellular migration and tissue remodeling, and elevated reactive oxygen species (ROS) caused by diabetes often leads to impaired blood flow, reducing the delivery of oxygen and nutrients to the wound site, hindering the healing process, and diabetic nerve damage also affects the normal signaling required for effective healing [3,4]. The altered microenvironment and abnormal collagen synthesis further contribute to the formation of non-healing wounds [5]. Moreover, the compromised immune function in diabetes renders individuals more susceptible to infections, exacerbating the challenge of chronic wound management [6]. The management of diabetic chronic wounds requires a multidisciplinary approach that combines advanced wound care techniques, infection control, glycemic control, and patient education [7]. Novel therapeutic interventions, such as versatile hydrogels and growth factors, are being explored to address the complexities of impaired wound healing in diabetes and improve prospects for successful wound

Peer review under responsibility of KeAi Communications Co., Ltd.
* Corresponding author.
** Corresponding author.
E-mail addresses: chenjianzuj4h@zju.edu.cn (J. Chen), tanweixxxx@zju.edu.cn (W.-Q. Tan).
[1] These authors contributed equally to this work.

https://doi.org/10.1016/j.bioactmat.2024.02.010
Received 19 October 2023; Received in revised form 24 January 2024; Accepted 7 February 2024

regeneration [8,9].

Hyaluronic acid (HA) is abundant in the extracellular matrix, where it contributes to tissue hydration, lubrication, and cellular activity [10–13]. Due to its biocompatibility and biodegradability, HA has found extensive applications in wound dressings and tissue engineering scaffolds. As a hydrogel wound dressing, its water retention capacity creates a moist environment that facilitates cell migration and growth within the wound site, ultimately promoting optimal wound healing [14]. This environment is essential for the formation of granular tissue, which supports re-epithelialization and collagen synthesis necessary for wound closure [15]. Collagen represents another major constituent of the skin's extracellular matrix with pivotal roles in wound healing. The regeneration process of wounds closely correlates with collagen synthesis [16]. With advancements in synthetic biology, recombinant human collagen has garnered increasing attention within the biomedical field [17]. Compared to animal-derived collagen sources, recombinant collagen offers superior biocompatibility, bioactivity, and enhanced safety profiles. Recombinant human type III collagen (rhCol) exhibits significant potential in the realm of wound repair and regeneration [16,18]. Both HA and type III collagen play indispensable roles as key components of the extracellular matrix during skin tissue remodeling processes and contribute significantly to efficient wound healing [19].

Dopamine (DA), a bioactive compound derived from marine mussels, has emerged as a promising agent in the field of wound dressing research [20,21]. Inspired by the ability of mussels to adhere to a variety of surfaces in aqueous environments, scientists have explored the unique adhesive properties of dopamine for potential wound healing applications. Thus, grafting DA to HA (HA-DA) through chemical crosslinking using 1-(3-Dimethylaminopropyl)-3-ethylcarbodiimide hydrochloride (EDC)/N-hydroxysuccinimide (NHS) will endow HA with excellent tissue adhesion and hemostatic properties. In addition, dopamine's intrinsic antioxidant and anti-inflammatory properties contribute to the reduction of oxidative stress and inflammation at the wound site, creating a favorable environment for efficient healing and minimizing the risk of infection. With the addition of rhCol, HA-DA@rhCol will play a better role in promoting wound repair, especially in chronic wound [22]. Thus, developing rhCol and HA-DA based injectable adhesive hemostatic antioxidant hydrogel wound dressing is highly anticipated in chronic wound management field, which has not been reported.

In this study, we synthesized HA-DA@rhCol hydrogel by employing oxidative coupling of the catechol group through an H_2O_2/HRP catalytic system, effectively combining the advantages of HA-DA and rhCol. The HA-DA@rhCol hydrogel exhibits exceptional properties, including elevated in vitro swelling, suitable degradation, tunable rheological behavior, remarkable adhesive properties, potent antioxidant activity, efficient hemostatic capability, enhanced photothermal effect, and NIR (near-infrared) irradiation-induced antibacterial behavior. Importantly, excellent blood compatibility and biocompatibility were also demonstrated in vitro to confirm the suitability of HA-DA@rhCol hydrogel for biomedical applications. To comprehensively evaluate the potential of this hydrogel for wound healing, we conducted several evaluations including wound closure studies, collagen metabolism analysis using immunohistochemical staining techniques as well as transcriptome sequencing in a diabetic rat model with full-thickness wounds. Collectively these findings highlight the promising effects of this versatile adhesive hemostatic hydrogel which possesses outstanding mechanical and rheological properties along with strong adhesion force capabilities while exhibiting antioxidant activity and NIR photothermal effects, thus making it highly suitable for wound healing applications.

2. Results and discussion

2.1. Preparation and characterization of HA-DA@rhCol hydrogel

A series of injectable hydrogels with adhesive hemostatic properties were prepared and evaluated for their mechanical and rheological properties, swelling ability, and adhesiveness to facilitate wound healing applications. The overall strategy for preparing HA-DA@rhCol hydrogels for wound healing is illustrated in Fig. 1. The selection of HA as the primary constituent of the hydrogels was based on its exceptional water-binding properties, which facilitate the creation of a moist wound environment and contribute to enhanced tissue regeneration and accelerated wound closure [23]. To confer HA with enhanced adhesiveness and antioxidant properties, the conjugation of DA to HA was achieved through EDC/NHS chemical crosslinking (Fig. 1). In the FTIR spectrum of HA-DA, a distinct absorption peak at 3084 cm^{-1} corresponding to the stretching vibration of the N–H bond in the DA benzene ring can be observed (Fig. 2A and Fig. S1, Supporting Information). The peak at 1557 cm^{-1} is likely attributed to the N–H bending vibration of the amide bond between HA and DA. Additionally, three consecutive vibrational absorption peaks within the range of 1190–1290 cm^{-1} are indicative of benzene ring vibrations in DA. The presence of those peaks provides conclusive evidence for the successful conjugation of the carboxyl group of HA and the amino group of DA through an amide bond. NMR analysis revealed that HA-DA exhibited characteristic signals corresponding to a benzene ring and methylene structure, confirming the successful coupling between HA and DA (Fig. S2, Supporting Information). In comparison with the hydrogen spectrum of HA, distinct chemical shifts were observed in the hydrogen spectrum of HA-DA at (i) 6.70 ppm, which corresponds to the proton peak of the benzene ring in the DA catechol group. Additionally, new proton peaks appeared at (ii) 3.08 ppm, (iii) 2.72 ppm, and (iv) 1.87 ppm due to adjacent methylene groups near the benzene ring. Furthermore, UV spectroscopy results for HA, HA-DA, and Dopamine provided further confirmation for successful synthesis of HA-DA (Fig. 2B). HA-DA solutions with concentrations of 0.5%, 1.0%, 1.5% and 2.0% (w/v) were prepared, and rhCol was added to each group at a final concentration of 50 μg/mL, resulting in the formation of hydrogel networks through oxidative coupling of catechol groups by using H_2O_2/HRP as an initiator system. The gelation time at 37 °C was measured, revealing that higher concentrations of HA-DA@rhCol resulted in shorter gelation times (Fig. 2C). Among them, the gelation time for the hydrogel pre-solution containing 0.5% HA-DA@rhCol exceeded 200 s at 37 °C, indicating it is not optimal for this formulation concentration. Conversely, the gelation time for the hydrogel pre-solution containing 2% HA-DA@rhCol was less than or equal to 25 s at this temperature, while providing poor needling performance and leaving short operation times for medical workers in general medical environments making it unsuitable as an optimal formulation concentration choice. Finally, we found that a concentration of 1.5% HA-DA@rhCol had a suitable gelation time about 30 s at 37 °C, which has almost the same gelation time as 1.5% HA-DA (Figure S3 Supporting Information).

2.2. Morphology, swelling, water retention, and degradation

By employing SEM to examine the microstructure of freeze-dried composite hydrogels with varying concentrations, including pore size and arrangement (Fig. 2D), interconnected porous structures were observed across all hydrogel groups. An increase in HA-DA concentration resulted in a reduction in hydrogel pore size. The average pore sizes for 0.5%, 1.0%, 1.5%, and 2.0% (w/v) HA-DA@rhCol composite hydrogels were measured as follows: 520.651 ± 85.278 μm, 384.197 ± 62.214 μm, 234.017 ± 59.157 μm, and 181.445 ± 64.675 μm respectively. Moreover, the increase in concentration resulted in a higher density of pores per unit area, accompanied by a more uniform distribution of pores. The swelling performance of hydrogels in tissue engineering is a crucial characteristic, thus the swelling behavior of hydrogels in PBS at 37 °C was observed. As shown in Fig. 2E, when hydrogel samples were immersed in PBS, all samples rapidly swelled within the first 2 h. Subsequently, all swelling curves gradually flattened and reached a state of equilibrium after approximately 24 h. The swelling rate showed an increasing trend with concentration due to the

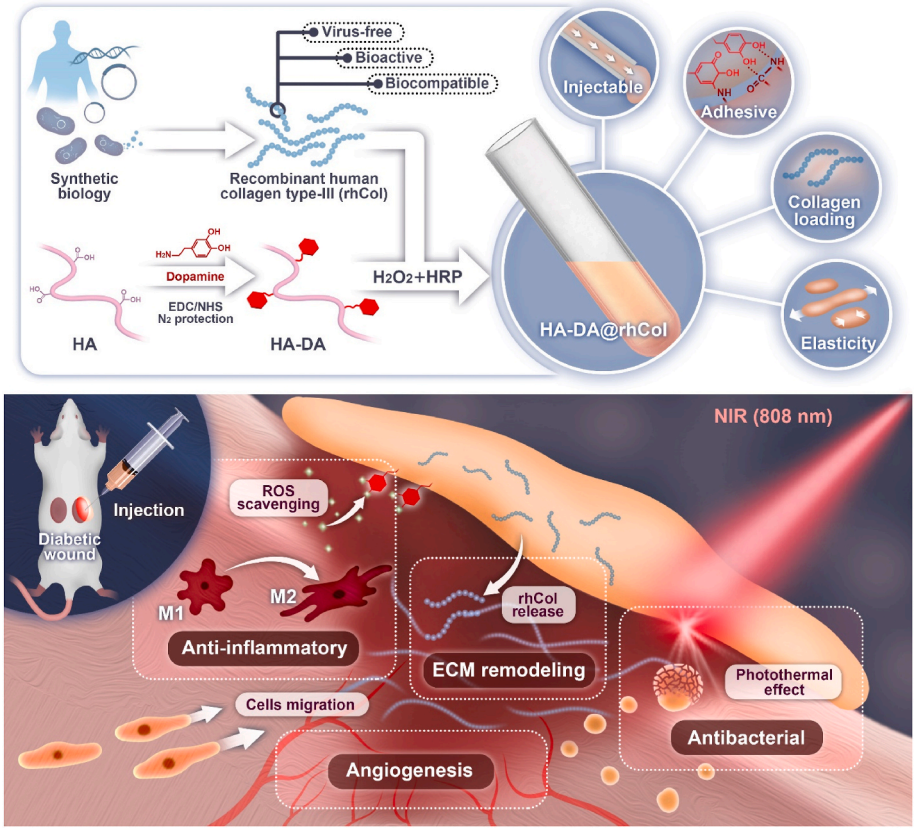

Fig. 1. Schematic illustration of HA-DA@rhCol hydrogel preparation and application for diabetic wound care in rat.

denser crosslinked network formed leading to higher water absorption capacity. These results indicate that HA-DA@rhCol hydrogel has suitable swelling ability, ensuring effective absorption of exudate when used as wound dressings. The water retention capacity of the hydrogel was tested using the weighing method. As shown in Fig. 2F, the water retention rate of the hydrogel is positively correlated with the concentration of HA-DA polymer. The water retention rates of 0.5% and 1.0% (w/v) HA-DA@rhCol composite hydrogels exhibited a significant decrease within three days, with water retention rates on day three being 19.70 ± 1.49% and 27.57 ± 1.24%, respectively. However, for 1.5% and 2.0% HA-DA@rhCol composite hydrogels, their water retention rates on day three were found to be 51.90 ± 1.44% and 57.40 ± 5 0.62%, respectively. The degradation curve of hydrogels in the presence of 1U/mL lysozyme is shown in Fig. 2G, and the 0.5% HA-DA@rhCol composite hydrogel had the fastest degradation rate, completely degrading by day 4. The degradation rates of the 1.0%, 1.5%, and 2.0% (w/v) HA-DA@rhCol composite hydrogels were 93.09 ± 3.15%, 90.06 ± 1.90%, and 74.72 ± 6.01% on day 16, respectively. The degradation of hydrogels in PBS (pH 5.5) were also tested, the rate of degradation is slightly slower than in lysozyme solution (Fig. S4).

A biomaterial with a pore size range of 100–300 μm is beneficial for facilitating oxygen and nutrient transport, promoting cell adhesion, synthesis of extracellular matrix, and ultimately aiding wound healing [24,25]. The results indicate a positive correlation between the water-holding performance of the hydrogel and HA-DA content. The HA-DArh@Col composite hydrogel containing collagen contains amino (-NH2) groups and DA with hydrophilic catechol groups enhanced the hydrophilicity of the hydrogels. After 3 days, it maintains a high-water content and exhibits superior enzymatic degradation stability. It degrades at an appropriate rate while keeping the wound environment moist, ensuring the integrity of the hydrogel and providing continuous protection to the wound site, thus avoiding frequent dressing changes.

2.3. Rheological and mechanical properties of HA-DA@rhCol hydrogel

The composite hydrogel can form continuous droplets during the injection process, and a 1 mL syringe can be used to continuously (Video S1) write the English font “ZJU” (Fig. S3D, Supporting Information). Rheological experiments can effectively demonstrate the injectability of the hydrogel. The relationship between viscosity and shear rate in the HA-DA@rhCol composite hydrogel was investigated using a rheometer. As shown in Fig. 3A, within the shear rate range of 1–100 s^{-1}, the viscosity decreases with increasing shear rate, indicating the hydrogel’s shear-thinning behavior and injectability. Viscosity plays a significant role in the pre-formulation and processing of biomedical materials. The initial viscosities of the 0.5%, 1.0%, 1.5%, and 2.0% (w/v) HA-DA@rhCol composite hydrogels are 0.388 Pa s, 9.31 Pa s, 22.0 Pa s, and 126.9 Pa s, respectively, showing concentration dependence. And The stability of hydrogel structure was studied in frequency scanning mode. When the G′ value is greater than the G″ value, it indicates that the hydrogel is in a gel state. As shown in Fig. S5 Supporting Information, in the frequency range of 0.1–10Hz, the G′ value of the four groups of hydrogels is always greater than the G “value, indicating that they have typical viscoelastic behavior, and the four concentrations of hydrogels can maintain their original hydrogel network structure in the middle and low frequency region.

Appropriate mechanical properties are essential for skin wound repair materials [26]. These properties not only ensure the material’s structural integrity but also promote effective adhesion, particularly when the skin tissue is subjected to external forces causing deformation. The compression stress-strain results of four concentrations of hydrogels can be seen in Fig. 3B. With the increasing in concentration of HA-DA, the mechanical properties of hydrogel HA-DA@rhCol can be effectively enhanced, showing higher stress at the same strain. Specifically, the stress increased from 36.2 to 46.3, 68.8 and 94.3 kPa at strain of about 80% along with the increase of concentration (w/v) of HA-DA

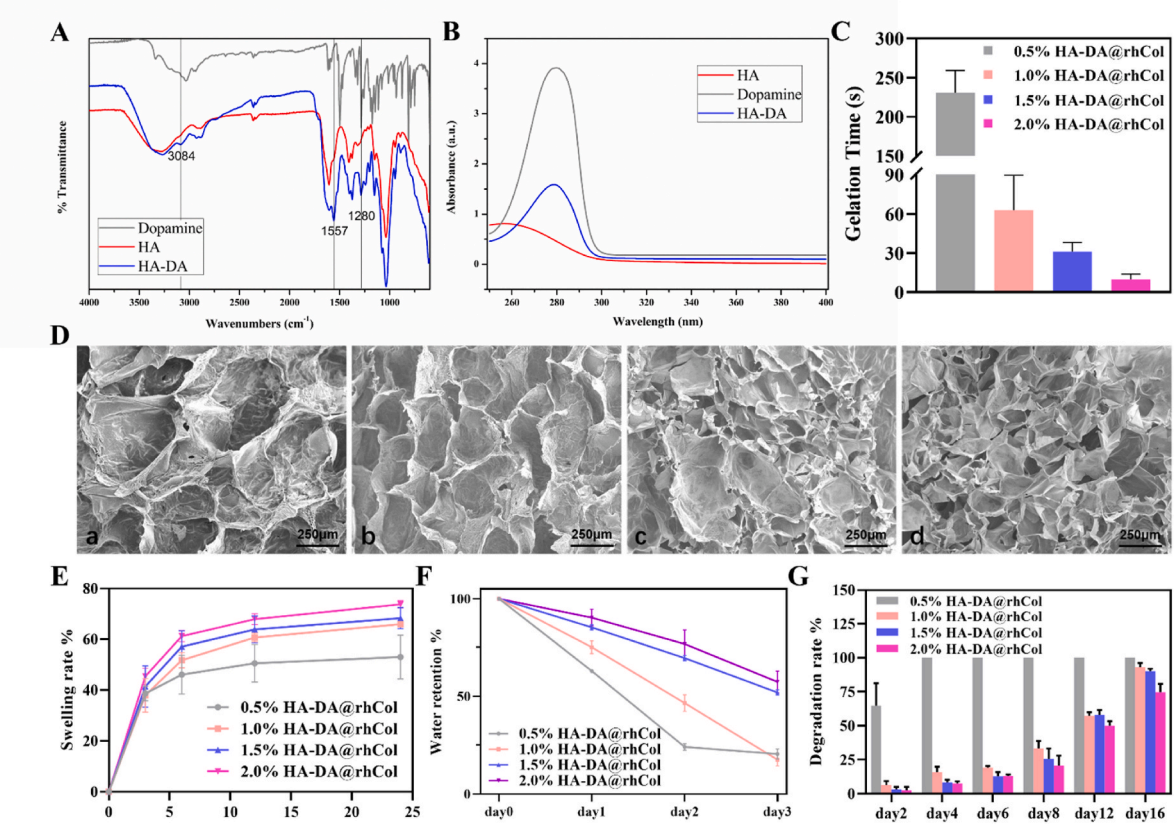

Fig. 2. Characterization of HA-DA@rhCol hydrogels. A) Full infrared spectrum and B) UV–Vis spectra of HA, HA-DA and Dopamine. C) Gelation time of HA-DA@rhCol with different HA-DA concentrations. D) SEM images of hydrogels, a. 0.5% HA-DA@rhCol; b. 1.0% HA-DA@rhCol; c. 1.5% HA-DA@rhCol; d. 2.0% HA-DA@rhCol. E) Swelling rate and F) Water retention and G) Degradation rate of hydrogels. (n = 3). Error bars indicated means ± SD.

from 0.5 to 1.0, 1.5 and 2.0%, respectively. (Video S2).

Furthermore, these hydrogels showcased remarkable stretchability (Fig. S6, Supporting Information), surpassing the extensibility range of human skin (typically 60–75%). The tensile testing outcomes for the four distinct hydrogel concentrations are depicted in Fig. 3C. It is evident that with escalating HA-DA concentrations, the elongation at break significantly improved, increasing from 85.0% to 157.9%, 189.7%, and ultimately 202.2%, respectively. Notably, the 2.0% HA-DA@rhCol formulation achieved the highest fracture strain. Concurrently, the tensile stress of the hydrogel experienced a parallel rise, elevating from 11.0 to 28.3, 52.2, and culminating at 71.5 kPa.

2.4. Adhesion and in vivo hemostatic performance of HA-DA@rhCol hydrogel

Functioning as exceptional wound dressings, these hydrogels not only exhibit a positive impact on the wound healing process through their active ingredients, but also demonstrate crucial adhesive performance [24,27]. To evaluate their adhesive capabilities, a lap-shear test was conducted to assess their bonding strength with skin tissue (Fig. 3D and E). Notably, all the hydrogels displayed robust adhesive strength. Notably, the 1.5% HA-DA@rhCol hydrogel exhibited the highest adhesive strength at 7.35 ± 1.45 kPa, great potential in wound management, surpassing that of standard commercial dressings (typically around 5 kPa). The remaining hydrogel concentrations resulted in adhesive strengths of 3.23 ± 0.28 kPa, 4.91 ± 0.90 kPa, and 5.46 ± 0.64 kPa, respectively. And there was no significant difference in adhesion between 1.5%HA-DA@rhCol group and 1.5% HA-DA group (Fig. S7, Supporting Information), Therefore the catechol group of HA-DA plays a major role in adhesion mechanism of these hydrogels.

In cases of skin trauma, particularly in scenarios involving full-thickness skin defects, the occurrence of bleeding becomes inevitable. Whether the bleeding could be stopped quickly plays a crucial role during the initial phase of the repair process [28]. As shown in Fig. 3G and H, it was demonstrated that these hydrogels possess the capability to firmly adhere to both skin surfaces and internal organs, encompassing the heart, liver, spleen, lung, and kidney. This adhesive quality further highlights the potential application of these hydrogels as effective hemostats. Therefore, a liver bleeding model was applied to ascertain the hemostatic ability of HA-DA@rhCol hydrogel. In Fig. 3F, the control group reached to approximate 574.6 ± 40.7 mg blood efflux from the liver of rat while only 202 ± 60.7 mg was observed in the 1.5% HA-DA@rhCol group, this disparity indicated that the hydrogel possessed remarkable hemostatic capacity in vivo.

2.5. Biocompatibility evaluation of HA-DA@rhCol hydrogel

Good biocompatibility is an important factor in the development of biomaterials. The blood compatibility of the hydrogel was evaluated through an in vitro hemolysis test [29], and the results are shown in Fig. 4A. It can be observed that all groups exhibited a pale-yellow color like the PBS group, with only slight hemolysis occurring. In contrast, the Triton X-100 group showed a bright red color, indicating a severe hemolytic reaction. Quantitative data from Fig. 4B (using Triton X-100 as positive control) also indicated that the hemolysis rates of all groups were below 5% of the hemolysis limit. The hemolysis rates for 1.5% HA, 1.5% HA-DA, and 1.5% HA-DA@rhCol were 0.33 ± 0.46%, 0.99 ± 0.72%, and 0.92 ± 0.58%, respectively. A hemolysis rate below 3% for polymeric materials is considered to demonstrate good biocompatibility. This suggests that the hydrogel does not disrupt the components in the blood and does not induce clotting or aggregation of platelets. Therefore, it can be safely used in the body.

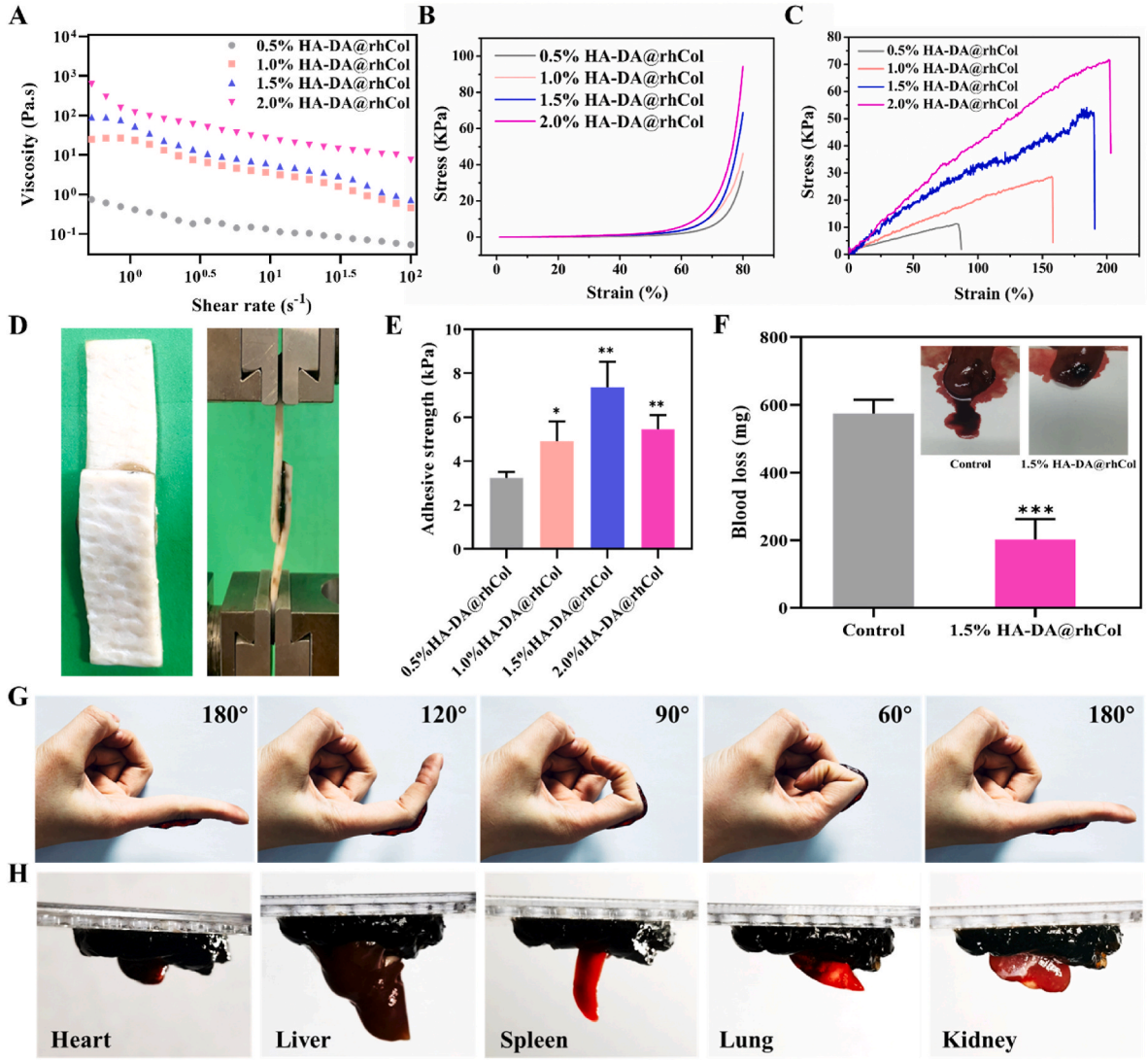

Fig. 3. Rheological and mechanical characterizations, adhesion and in vivo hemostatic performance of HA-DA@rhCol hydrogels. A) Shear rheology and B) Stress-strain profiles of these hydrogels by compression. C) Stress-strain profiles of these hydrogels by tensile tests. D) Photographs of adhesive strength test, E) Adhesive strength of different hydrogels, n = 3. F) Hemostatic performance of hydrogel HA-DA@rhCol. G) Photographs of hydrogels sticking to fingers. H) Photographs of hydrogels glued to different organs. Error bars indicated means ± SD. Statistical significances were analyzed using *t*-test. *P < 0.05, **p < 0.01, ***p < 0.001 compared with control group.

As depicted in Fig. 4C, most NIH-3T3 cells cultured with the 1.5% HA, 1.5% HA-DA, and 1.5% HA-DA@rhCol composite hydrogel survived (indicated by green color), with hardly any observed cell death. Moreover, the cell growth morphology remained unchanged, and a higher fluorescence density was observed in the 1.5% HA-DA@rhCol group (Fig. 4C and d). To assess the hydrogel's cytotoxicity and proliferative effect on NIH-3T3 cells, the MTT assay was conducted. As illustrated in Fig. 4D, there was no significant difference in the proliferation rate among the hydrogel groups on the first day. However, on the second and third days, the 1.5% HA-DA@rhCol composite hydrogel showed a significantly higher proliferation rate compared to the 1.5% HA and 1.5% HA-DA groups ($P < 0.05$). This finding suggests that collagen promotes the proliferation of NIH-3T3 cells to some extent. In conclusion, the 1.5% HA-DA@rhCol composite hydrogel demonstrated excellent cell compatibility without any cytotoxic effects. We also demonstrated the in-vivo biocompatibility of the hydrogels, with no significant pathological damage found in the major organs of the rats after treatment with each set of hydrogels (Fig. S8, Supporting Information).

2.6. Antioxidant and anti-inflammation ability of HA-DA@rhCol hydrogel

The existence of reactive oxygen species (ROS) in wound site can lead to oxidative stress, which will damage cellular structures, including proteins, lipids, and DNA, leading to further tissue damage and impaired healing [29,30]. Research investigating the application of materials possessing free radical scavenging properties on patients or animals has shown considerable enhancements in wound healing. We assessed the in vitro antioxidant capacity of hydrogels through the DPPH radical scavenging assay. As shown in Fig. 5A and B, it demonstrates that 1.5% HA exhibits antioxidant properties, but both 1.5% HA-DA and 1.5% HA-DA@rhCol hydrogels exhibit significantly superior antioxidant capabilities. The impact of hydrogels on the reducing intracellular ROS co-incubating Raw264.7 macrophages was quantitatively analyzed through flow cytometry (Fig. 5C and D). In the negative control group, the ROS release was relatively low, after H_2O_2 induction, the percent of ROS positive cells significantly increased, upon incorporating 1.5% HA-DA and 1.5% HA-DA@rhCol composite hydrogel scaffolds, the ROS-positive cell rates notably decreased.

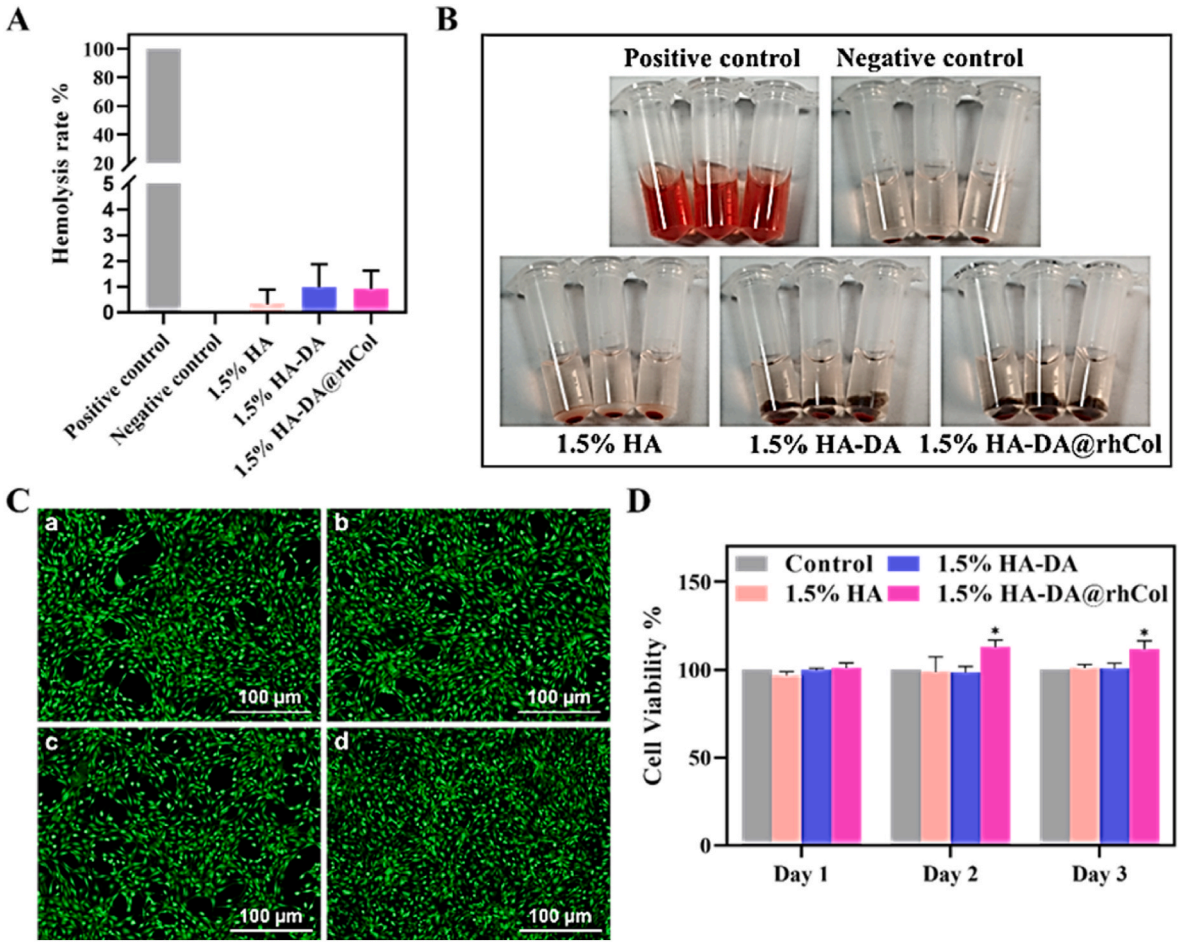

Fig. 4. Cell compatibility of HA-DA@rhCol hydrogels. A) Hemolysis rate of HA-DA@rhCol hydrogel. B) pictures of Hemolysis. C) Dead/live staining of a. Control, b. 1.5% HA, c. 1.5% HA-DA, d. 1.5% HA-DA@rhCol. D) Cell viability detected by MTT of NIH3T3 co-cultured with the hydrogels. Error bars indicated means ± SD. Statistical significances were analyzed using *t*-test. *P < 0.05 compared with control group.

Then, The DCFH-DA probe was used to label the intracellular ROS levels of cells cultured with different hydrogels, evaluating their antioxidant capacity under CLSM observation. The results also demonstrated that the intensity of cells dyed in 1.5% HA-DA and 1.5% HA-DA@rhCol respectively treated group decreased significantly compared with those of blank controls and 1.5% HA treated group. In conclusion, HA-DA and HA-DA@rhCol composite hydrogels effectively attenuated intracellular oxidative stress, promoting the maintenance of intracellular redox balance.

Immune dysregulation also disrupts the natural process of wound healing, and persistent pro-inflammatory responses are the hallmark of chronic wounds [31]. Manipulating the immune microenvironment stands out as a promising strategy for the treatment of such chronic wounds. Within the wound site, M1 macrophages are responsible for generating pro-inflammatory cytokines, while their M2 counterparts adopt an anti-inflammatory phenotype, releasing mediators that soothe inflammation. Polydopamine (PDA) has been recognized as a remarkable regulator of macrophage due to its exceptional biocompatibility and its capacity to promote the transition of macrophages towards M2 polarization. To further substantiate this, we next validated the immunomodulatory properties of 1.5% HA-DA@rhCol. CD86, a surface molecule expressed on M1 macrophages, exhibited a significant reduction in expression within the 1.5% HA-DA@rhCol group (Fig. 5F). These results suggest that 1.5% HA-DA@rhCol not only has ability of ROS scavenging but also actively promotes M2 macrophage polarization.

2.7. Photothermal and antibacterial properties of HA-DA@rhCol

A chronic wound infection is very common clinically, and such an infection could lead to even more challenging wound healing. Therefore, the development of an antibacterial hydrogel is still highly necessary [32,33]. Dopamine possesses excellent photothermal effects, which can convert light into heat energy, and the heat energy that continues to accumulate can effectively inhibit bacteria after a certain temperature and time. Therefore, we tested the photothermal abilities of hydrogels, 1.5% HA, 1.5% HA-DA and 1.5% HA-DA@rhCol, they were irradiated with an 808 nm laser at 2.0 W cm^{-2} for 5 min. As shown in Fig. 6A, 1.5% HA-DA and 1.5% HA-DA@rhCol both have excellent photothermal effect, the highest temperature of them could reach about 80 °C after 5 min irradiation. Subsequently, we irradiated 1.5% HA-DA@rhCol with laser at 2.0 W/cm^{-2}, 1.5 W/cm^{-2}, 1.0 W/$cm^{-2}$and 0.5 W/cm^{-2} and recorded their temperature changes within a 5 min period. As the intensity decreased, the temperature of the hydrogel after 5 min of irradiation decreased from around 80 °C to approximately 60 °C, 50 °C and 40 °C, respectively. Furthermore, the 1.5% HA-DA@rhCol hydrogel exhibited remarkable photothermal stability even after undergoing numerous cycles of alternating near infrared ray (NIR) irradiation. This was evident from the absence of any notable reduction in the maximum heating temperature (Fig. 6C). Those results show that the 1.5% HA-DA@rhCol hydrogel has outstanding photothermal performance. Then, we investigated the in vitro antibacterial efficacy of the 1.5% HA-DA@rhCol hydrogel against two predominant bacterial strains: Gram-negative *E. coli* and Gram-positive *S. aureus*, commonly associated

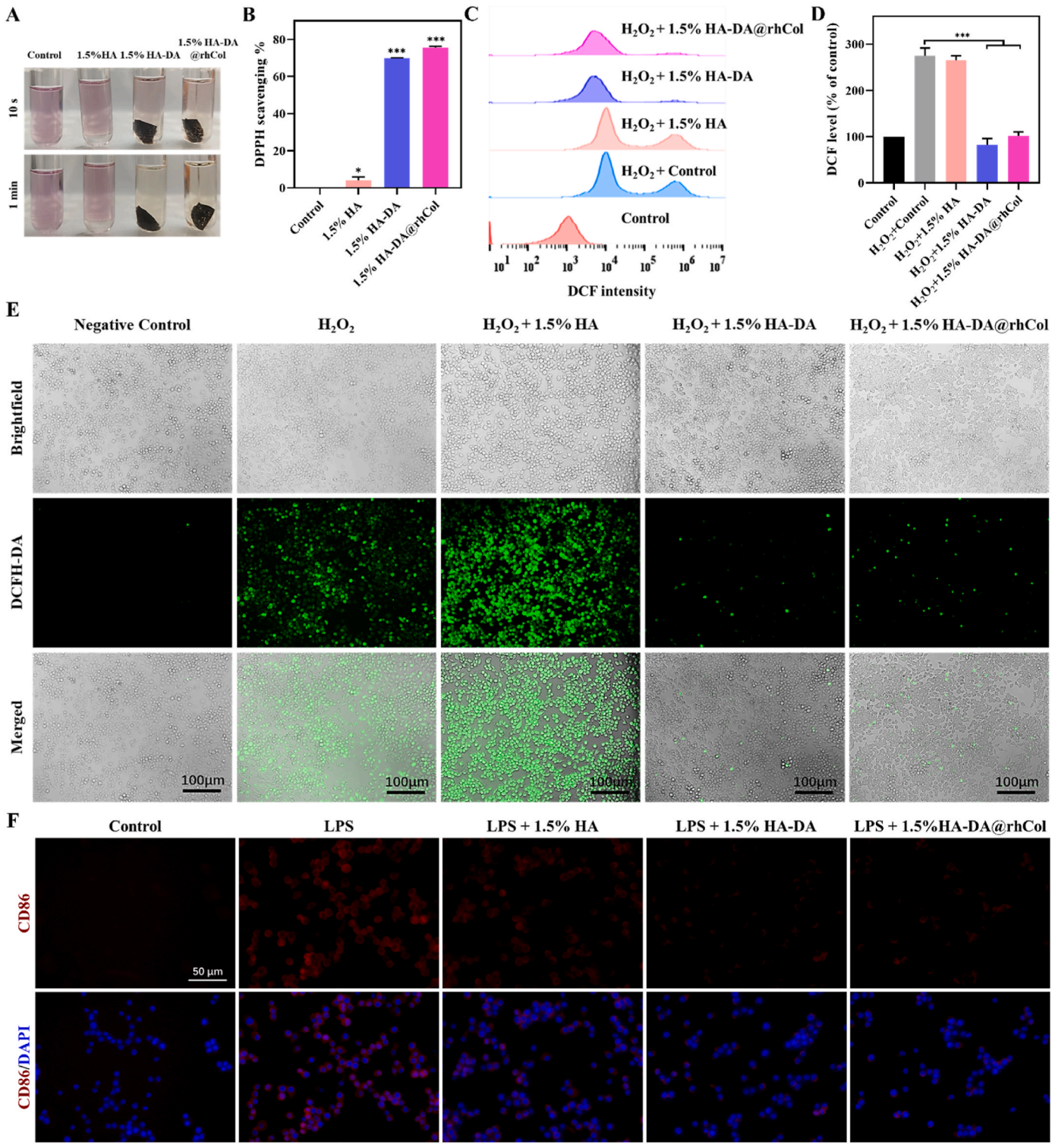

Fig. 5. Antioxidant efficiency and inflammation control of hydrogels. A) The images of DPPH scavenging of all groups for 10 s and 1 min and B) DPPH scavenging capabilities by 1.5% HA, 1.5% HA-DA and 1.5% HA-DA@rhCol, n = 3. C) and D) Flowcytometry of DCFH-DA labeled Raw264.7 cells in fluorescein isothiocyanate FITC-A channel in different group, n = 3. E) Intracellular ROS-scavenging performance of 1.5% HA, 1.5% HA-DA and 1.5% HA-DA@rhCol. F) Fluorescence images of RAW 264.7 cells after treatment with LPS (control) or LPS + 1.5% HA, 1.5% HA-DA and 1.5% HA-DA@rhCol. CD86: M1 macrophages. Error bars indicated means ± SD. Statistical significances were analyzed using *t*-test. *P < 0.05, ***p < 0.001 compared with control group.

with various infectious diseases. As shown in Fig. 6D and the quantitative results of clone formation rate (Fig. S9, Supporting Information), after NIR at 1.5 W cm^{-2} irradiation for 30 min, 1.5% HA-DA and 1.5% HA-DA@rhCol presented obvious antibacterial effect. The results of SEM also showed that the cell wall of bacteria was broken under the action of photothermal effect.

2.8. Promotion of cell migration and angiogenesis

Collagen protein plays a pivotal role in tissue regeneration by

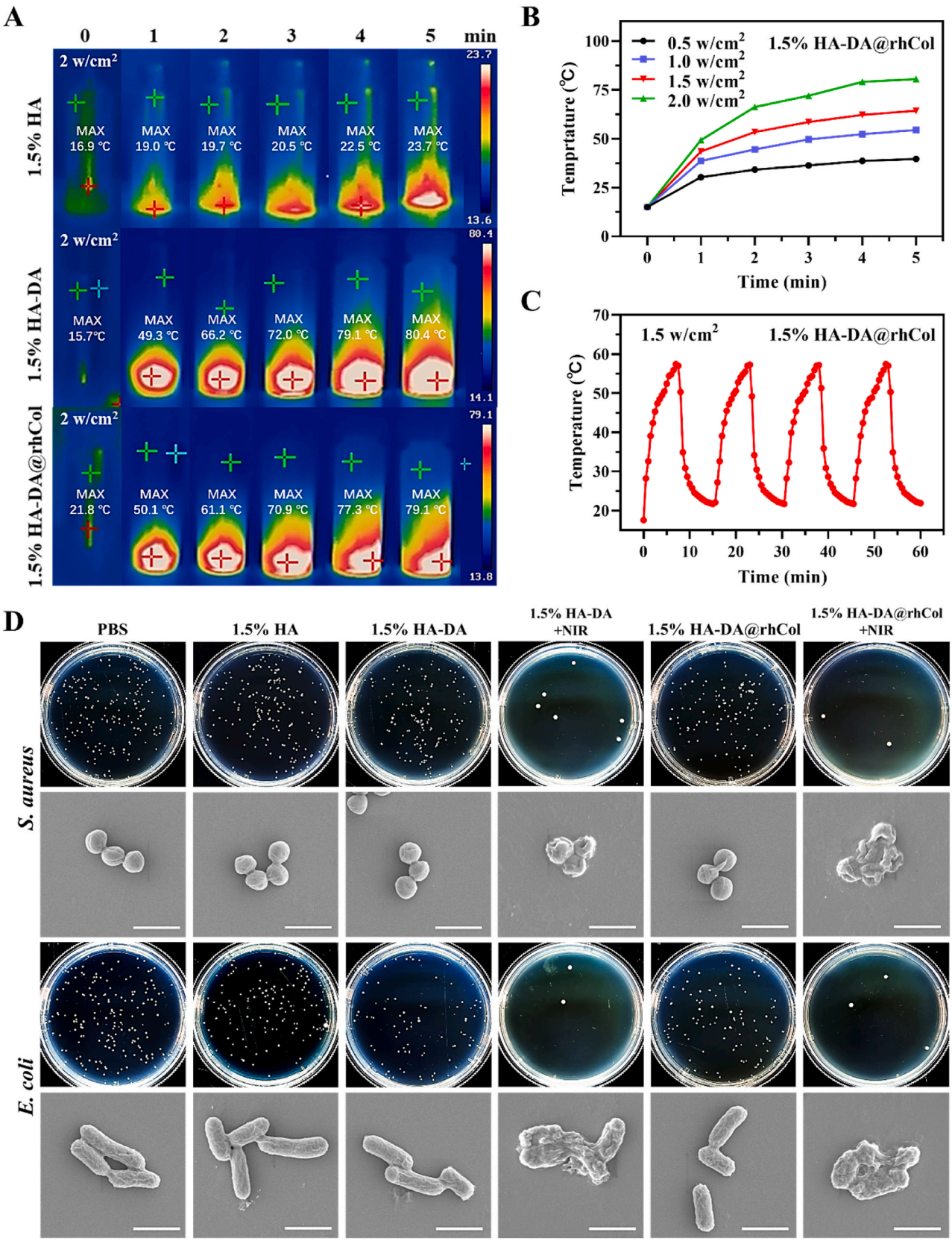

Fig. 6. Photothermal effect and antibacterial activity of hydrogels. A) Real-time infrared thermal images of 1.5% HA, 1.5% HA-DA and 1.5% HA-DA@rhCol, and B) photothermal curves of 1.5% HA-DA@rhCol under laser power intensity, n = 3. C) Photothermal curves of 1.5% HA-DA@rhCol under 1 W/cm^{-2} in four on/off cycles, n = 3. D) Colony formation and SEM photograph (bar = 1.5 μm) of *S. aureus* and *E. coli*. Bacteria were cocultured with various concentrations of the Fe/PDA@GOx@HA, irradiated with or without an 808 nm laser at 1 W cm^{-2} for 30 min.

influencing various aspects of the process [34]. It significantly impacts cell migration, facilitating the movement of cells to the injured or damaged site. Additionally, collagen promotes angiogenesis, the formation of new blood vessels, which is crucial for supplying nutrients and oxygen to regenerating tissues [35]. Incorporating human recombinant collagen type-III (rhCol) into the HA-DA@rhCol hydrogel, we assessed its potential to enhance in vitro cell migration (HaCaT) and angiogenesis (HUVEC). First, the scratch assays of HaCaT were performed to assess the cell migration rate under co-cultured with or without different hydrogels. As shown in Fig. 7A, 1.5% HA-DA@rhCol has most remarkable performance of promoting cell migration of HaCaT, the gap between HaCaT cells was closed at 24 h after scratching compared to other groups. The migration rate of HaCaT in the 1.5% HA group, 1.5% HA-DA group and 1.5% HA-DA@rhCol group was 46.9 ± 8.0%, 39.9 ± 4.7% and 99.0 ± 0.4%, respectively, which was statistically significant compared with control group (18.8 ± 7.0%) (Fig. 7C).

The promotion of vascular regeneration of wound tissue is the key to the treatment of chronic wound that lack nutrients. Therefore, we evaluated whether the hydrogel has the effect of promoting vascular regeneration of vascular endothelial cells through tube formation experiments. The results showed that 1.5%HA-DA@rhCol hydrogel had the most significant effect on promoting tube formation of HUVEC cells, as shown in Fig. 7B, the number of tubes in 1.5% HA group, 1.5% HA-DA group and 1.5% HA-DA@rhCol group was 36.2 ± 2.8, 33.8 ± 6.5 and 46.8 ± 1.8, respectively, which was statistically significant compared with control group (19.8 ± 3.6) (Fig. 7D). The good bioactivity of the hydrogel in promoting cell migration and vascular regeneration shows that it can be used as a good dressing for chronic wound repairing.

2.9. Evaluation of in vivo diabetic wound repairing in rat

For a more comprehensive assessment of its potential in chronic wound healing, we conducted an in vivo test using a diabetic rat model with full-thickness skin defects that was created by high fat diet, streptozotocin (STZ) injection and creating a 10-mm diameter incisional wound on dorsum of diabetic rats. This test aimed to confirm the benefits of utilizing HA-DA@rhCol as a wound dressing. The 1.5% HA-DA@rhCol hydrogel, which demonstrated optimal performance in previous assessments, was selected as a representative. A Tegaderm dressing served as the control group. Wound observations and photography were conducted on days 0, 3, 7, 11, and 15 (Fig. 8A and B). Notably, the 1.5% HA-DA@rhCol hydrogel displayed the most significant efficacy in promoting diabetic wound healing. Histological examination of wound samples taken on day 11 revealed that 1.5% HA-DA@rhCol exhibited superior outcomes in terms of re-epithelialization, granulation tissue formation, and tissue remodeling (Fig. 8C). The quantitative outcomes illustrated in Fig. 8F and G highlighted that, on Day 11, the wound closure rate and wound length rate of 1.5% HA-DA@rhCol outperformed those of the 1.5% HA and control groups. This underscores the positive impact of rhCol on diabetic wound healing, with the rates of 1.5% HA-DA@rhCol consistently leading the pack among these groups.

In the phase of skin wound remodeling, the deposition of collagen is a crucial process and serves as a benchmark for evaluating wound healing. Different types of collagen fibers are present, notably types I and III. Type I collagen constitutes the primary component of skin, contributing to its thickness, while type III collagen is finer and forms the framework of reticular fibers. Masson's trichrome stain and sirius red staining were used to detect deposited collagen. Therefore, the

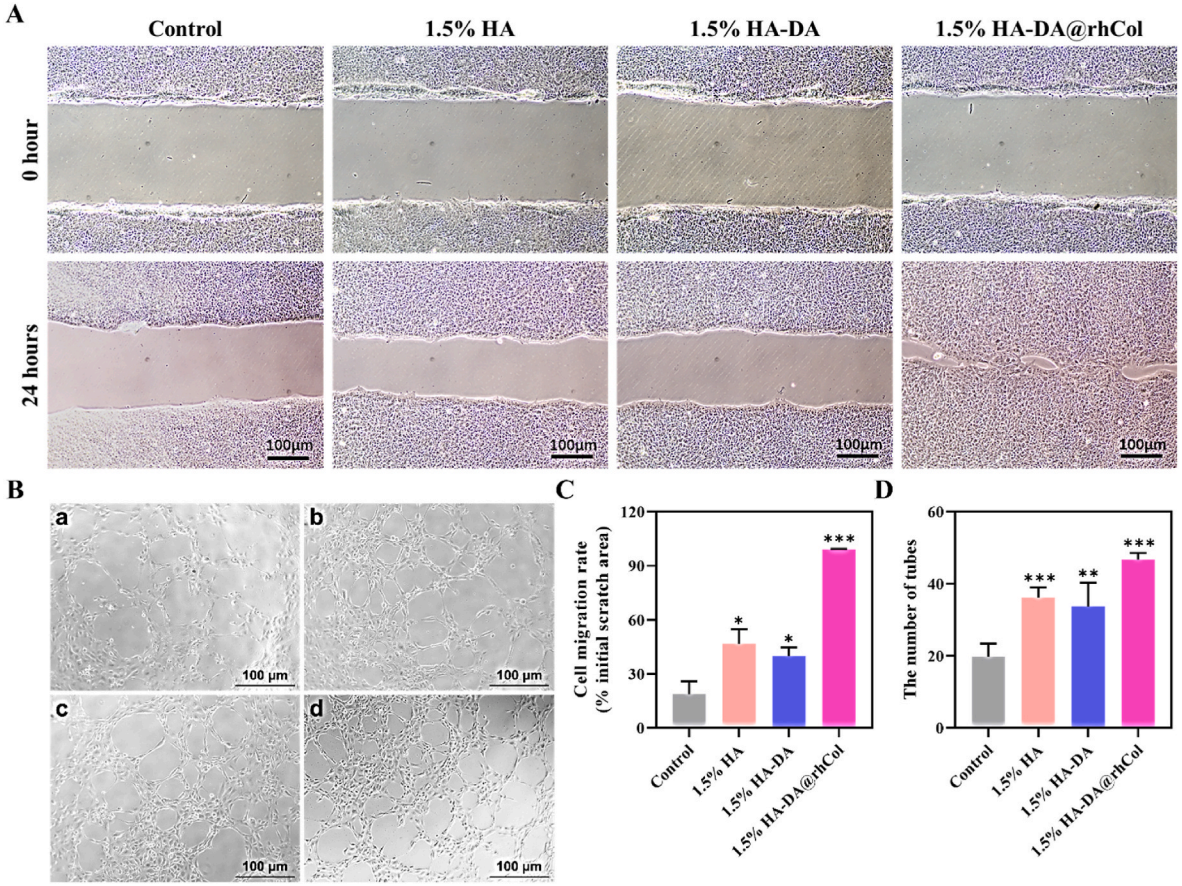

Fig. 7. Cell migration and angiogenesis of hydrogels. A) Scratch test of HaCaT cells and B) Tube formation of HUVECs co-cultured with 1.5% HA, 1.5% HA-DA and 1.5% HA-DA@rhCol. C) and D) Quantitative analysis of cell migration and tube formation, n = 3. Statistical significances were analyzed using *t*-test. *P < 0.05, **p < 0.01, ***p < 0.001 compared with control group.

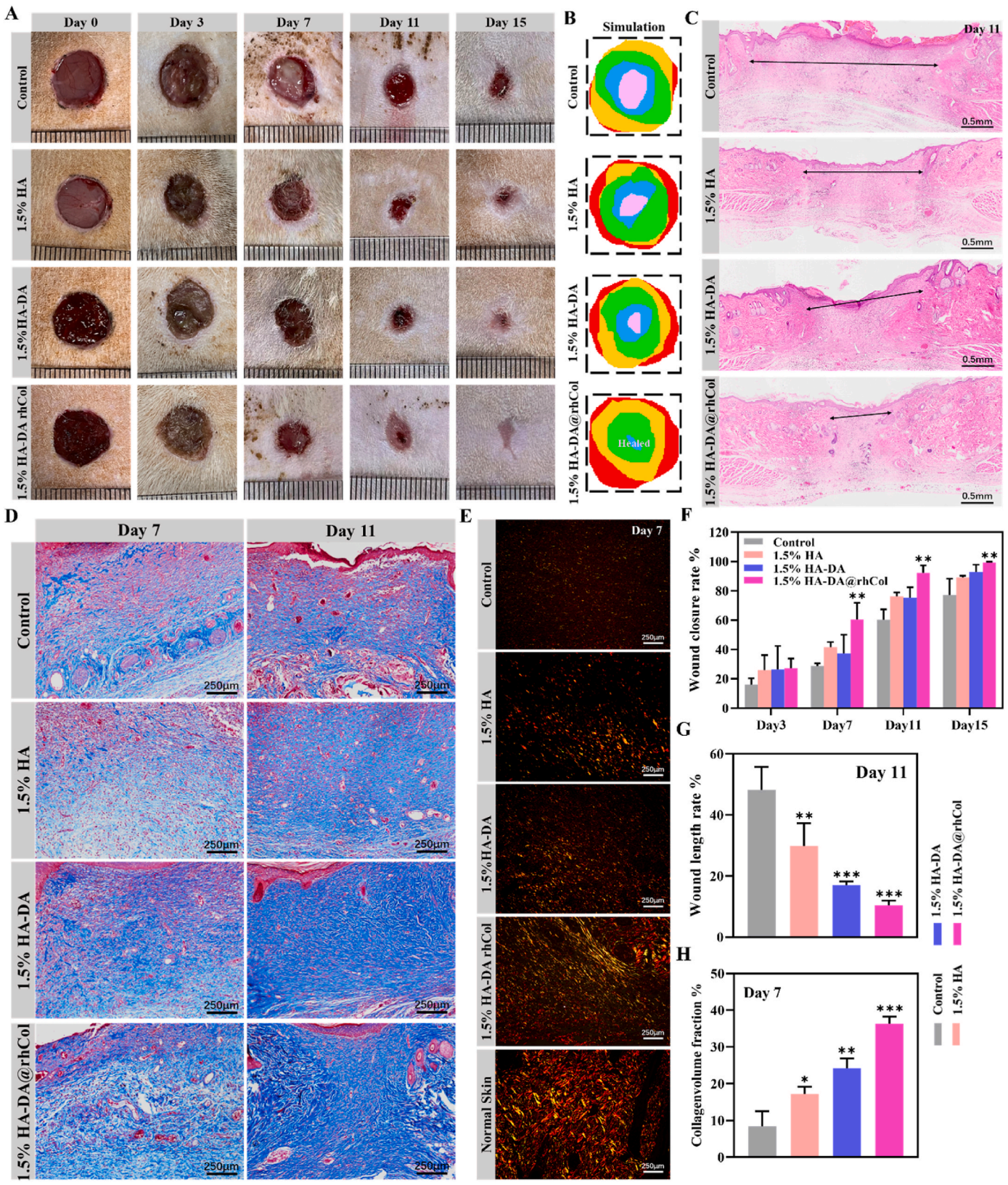

Fig. 8. Treatment efficiency of the chronic wound by 1.5% HA-DA@rhCol in diabetic rat. A) Representative photographs of the diabetic chronic wound treated with different dressing. (B) Simulation plots of wound closure. C) H&E staining of the wound indicated the healing condition at 11 days. D) Masson's staining and E) Sirius red staining of the wound sections at day 7 and day 14. F) The quantitative analysis of wound closure, G) wound length in H&E staining and H) collagen volume fraction in Masson's staining. n = 3. Statistical significances were analyzed using *t*-test and one-way ANOVA. *P < 0.05, **p < 0.01, ***p < 0.001 compared with control group.

results of masson' trichrome stain indicated that the group of 1.5% HA-DA@rhCol had less keratin-positive area at day 7 and had more thicker collagen fibers at day 11 than 1.5% HA-DA group, 1.5% HA group and control group, and there was a statistically significant difference in their area (Fig. 8H). The results of sirius red staining also demonstrated that 1.5% HA-DA@rhCol remarkably promote the production of type I collagen in the wound tissue at day 7 (Fig. 8E).

2.10. The potential mechanism of accelerated diabetic chronic wound healing

We have proved that HA-DA@rhCol hydrogel has a good effect on promoting chronic wound healing through a rat diabetic wound model, so we also need to explore its mechanism of promoting wound healing in vivo. Using an immunofluorescence assay on tissue sections, we assessed the presence of F4/80 and CD206 markers for M2 macrophages in the initial wound granulation tissue on day 3. The findings, depicted in Fig. 9A, reveal a notable enhancement in the M2 macrophage ratio due to the application of the 1.5% HA-DA@rhCol hydrogel. This improvement is evident in the increased CD206 expression among F4/80 positive cells (Fig. 9C).

Following the inflammatory phase of wound healing, we proceeded to assess F4/80 expression in wound tissues on day 11 using immunohistochemistry staining (Fig. 9B and D). During this stage, the group treated with 1.5% HA-DA@rhCol hydrogel displayed a noticeable reduction in inflammatory response within the wound tissue, in contrast to the control and other groups. Simultaneously, the immunohistochemical analysis of CD31 protein demonstrated the effective promotion of vascular regeneration in wound tissue by the rhCol in the hydrogel (Fig. 9B and E).

To delve deeper into the underlying mechanisms driving the accelerated wound healing facilitated by HA-DA@rhCol, we conducted a transcriptomic analysis with the samples collected from both the control and the 1.5% HA-DA@rhCol group. The results highlighted notable differences in gene expression across the groups, with 205 genes showing increased expression and 109 genes showing decreased expression as indicated in the volcano plots and heatmap (Fig. 10A and B). The genes that displayed altered expression were analyzed using the Gene Ontology (GO) database. This analysis encompassed biological processes (BP), cellular components (CC), and molecular functions (MF). The up-regulation of genes associated with epidermis development and skin development in the HA-DA@rhCol group, as depicted in Fig. 10C, demonstrates the promotion of re-epithelialization of diabetic wounds by the hydrogel. Additionally, the hydrogel increased the expression of genes involved in positive regulation of angiogenesis and vasculature development to enhance vascular regeneration within wound tissue. Furthermore, there was an augmentation in gene expression related to collagen extracellular matrix formation. Conversely, terms associated with cell number homeostasis, basal plasma membrane and oxygen transport were downregulated, which indicates that the wound tissue was in a relatively stable state with sufficient nutrient supply after hydrogel treatment. Furthermore, we explored potential signaling pathways using the Kyoto Encyclopedia of Genes and Genomes (KEGG). As seen in Fig. 10E and F, diabetic wound healing in the HA-DA@rhCol group showed changes in MAPK signaling, PI3K-Akt signaling, and IL-17 signaling. These pathways are associated with the regulation of chronic inflammation. Collectively, these results demonstrate that the HA-DA@rhCol hydrogel accelerated diabetic chronic wound healing through promoting skin regeneration pathways and regulating pro-inflammatory pathways.

3. Conclusion

In our research, we successfully created a range of mussel-inspired HA-DA@rhCol hydrogels. These hydrogels offer injectability, adhesive properties, hemostatic capabilities, photothermal antibacterial effects, and antioxidant properties that help regulate inflammation. The hydrogel component contains natural biopolymers such as rhCol and HA, imparting superior biocompatibility and promoting cell proliferation and migration. Through a series of experiments, we comprehensively evaluated the porosity, swelling behavior, degradation rate, rheological properties, and mechanical strength of the hydrogels. Among them, the 1.5% HA-DA@rhCol hydrogel exhibited optimal physical and chemical characteristics for wound dressings. Inspired by mussel-derived catechol groups, these hydrogels demonstrate exceptional adhesive and hemostatic qualities while also possessing potent antioxidant abilities that enhance the anti-inflammatory effects of hyaluronic acid. Moreover, our hydrogel effectively scavenges reactive oxygen species (ROS), thereby mitigating oxidative stress in chronic wound tissues. By incorporating recombinant human collagen type-III (rhCol), these hydrogels acquire the ability to provide essential nutrients for skin wound regeneration. This capability was confirmed through in vitro scratch and tube formation assays as well as in vivo testing on diabetic rat models with wounds; our results demonstrated that the HA-DA@rhCol hydrogel promotes diabetic wound healing by accelerating cell migration, enhancing angiogenesis, controlling inflammation levels, and facilitating collagen fiber deposition. Indeed, the mechanical properties and adhesive ability can be enhanced to broaden its application scope, such as in the treatment of myocardial infarction. Collectively, these findings underscore the immense potential of this versatile hydrogel formulation in expediting diabetic chronic wound healing processes.

4. Methods and materials

4.1. Materials

Hyaluronic acid (MW 40 kDa–140 kDa) and dopamine hydrochloride were purchased from Yuanye Bio (Shanghai China), recombinant human type III collagen were provided by Jland Biotech (Jiangsu China). 1-ethyl-3-(3-dimethylaminopropyl) carbodiimide hydrochloride (EDC-HCl) and N-hydroxysuccinimide (NHS) were purchased from Aladdin (Shanghai China). DCFH-DA probe, Calcein AM and propidium iodide were purchased from Solarbio (Beijing, China) Dulbecco's modified Eagle's medium (DMEM), fetal bovine serum (FBS) and 40,6-diamidino-2-phenylindole (DAPI) were supplied by Thermo Fisher Scientific. F4/80, CD86, CD206, CD31 antibodies were purchased from Proteintech (Wuhan, China).

4.2. Synthesis of hyaluronic acid-dopamine and recombinant human type III collagen (HA-DA@rhCol)

To prepare the HA-DA conjugate, a total of 1.0 g of hyaluronic acid (HA) was completely dissolved in 100 mL of deionized water. The resulting HA solution was then kept under a nitrogen environment. Subsequently, 1.48 g of EDC-HCl and 0.9 g NHS were slowly added to the HA solution with vigorous stirring for 20 min. Following that, 1480 mg of dopamine (DA) was added to the solution. The pH of the solution was adjusted to a range between 5.0 and 5.5 and allowed to react for 8 h. The final solution obtained from the reaction was then divided into dialysis bags with a molecular weight cut-off of 8000–14000 Da. The dialysis was performed in pure water for 48 h to completely remove unreacted reagents and salts. The resulting dialyzed solution was freeze-dried, then HA-DA scaffold was measured using a Fourier Transform Infrared Reflection (FTIR) spectrometer (Nicolet iS50, Thermo Fisher). The catechol content was detected by UV–vis spectrometer (PerkinElmer Lambda 35), measuring absorbance at 280 nm. The liquid 1H NMR test of HA-DA was carried out with a nuclear magnetic resonance hydrogen spectrometer (Bruker Avance II).

Then to prepare HA-DA@rhCol, and 0.05 g, 0.10 g, 0.15 g and 0.2 g HA-DA freeze-dried foams were added to 7.5 mL PBS solution at room temperature and stirred until completely dissolved to obtain HA-DA

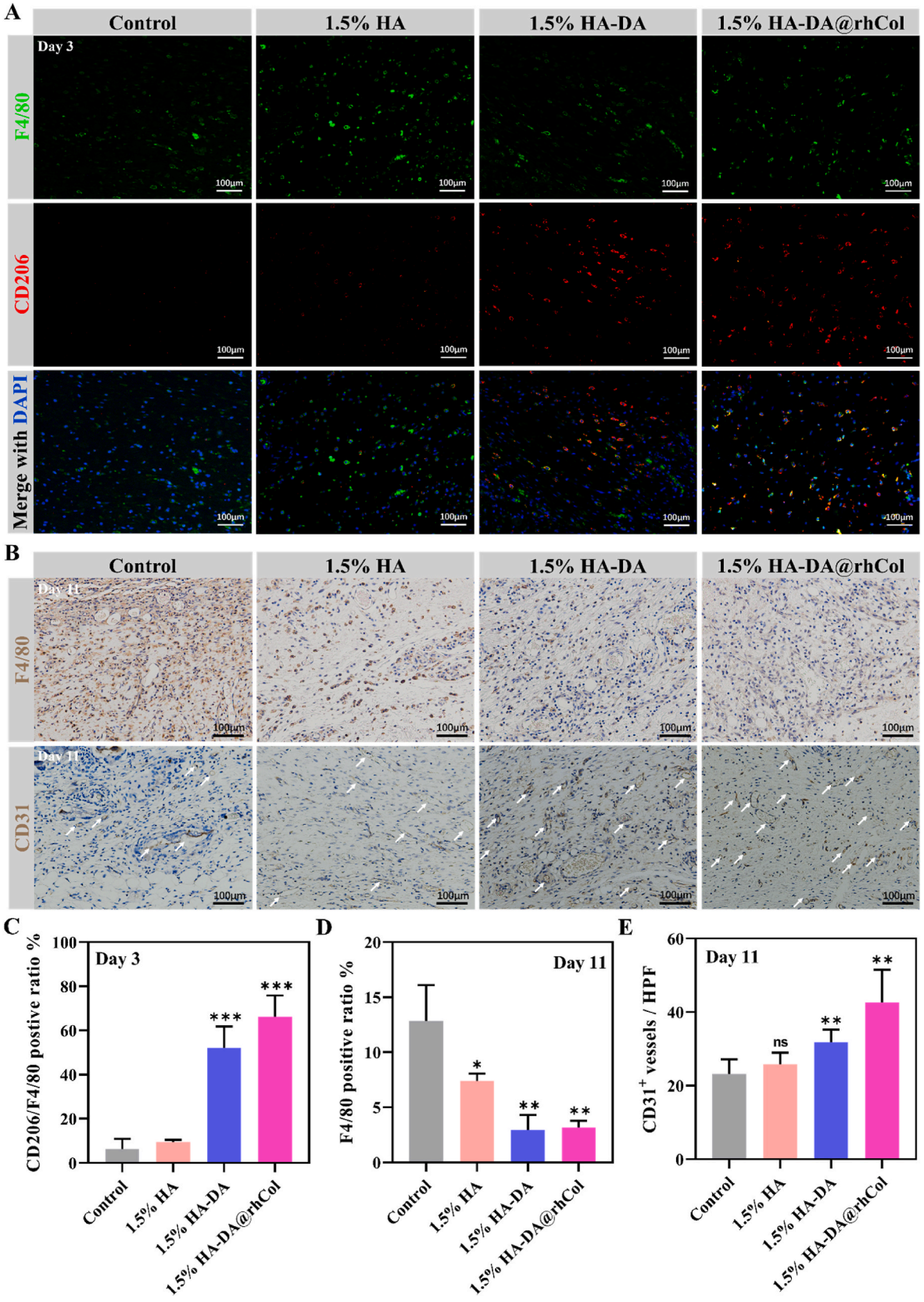

Fig. 9. Modulation of inflammation microenvironment and regeneration in diabetic wound. A) Immunofluorescence images of marker F4/80 (Green) and CD206 (Red) in wound tissue, and nuclei were stained with DAPI (blue). B) Immunohistochemistry staining of F4/80 and CD31 on the wound sections at day 11. C) Quantitative analysis of CD206 fluorescence intensity/F4/80 fluorescence intensity ratio. D) and E) Quantitative analysis of F4/80 and CD31 positive area at day 11, respectively. Statistical significances were analyzed using one-way ANOVA. *P < 0.05, **p < 0.01, ns, p > 0.05 compared with control group.

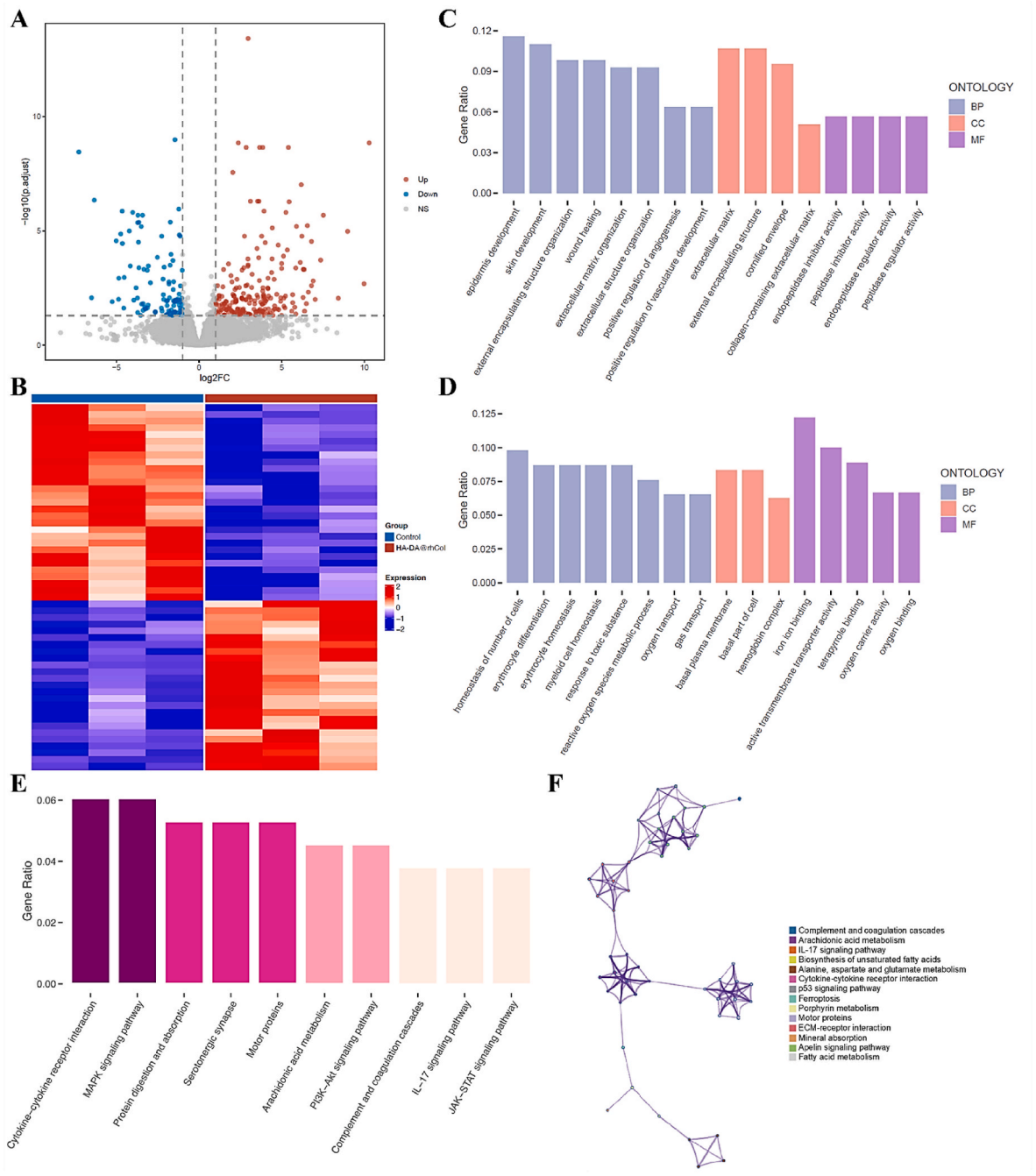

Fig. 10. Mechanistic analysis of wound healing with HA-DA@rhCol treatment. A) Volcano plot of transcriptomic analysis of differentially expressed genes (n = 3 biologically independent samples). B) Heatmap analysis of differentially expressed genes. C) and D) GO analysis of differentially up-regulated and down-regulated expressed genes. E) and F) Enriched KEGG pathways of HA-DA@rhCol versus Control. The size of the dots indicates the number of genes associated with indicated KEGG terms.

precursor solutions with different concentrations. The HA-DA@rhCol composite hydrogel with final concentrations of HA-DA of 0.5%, 1.0%, 1.5% and 2.0% (w/v) was prepared by adding 1 mL rhCol solution (0.5 mg/mL) 1 mL HRP (0.25 M), and 0.5 mL H_2O_2 (0.1 M), then stirring well, respectively. HRP/H_2O_2 was used to produce enzymatic reaction.

4.2.1. Scanning electron microscope (SEM)

First, the hydrogel was cut and freeze-dried for 48 h, and then the freeze-dried hydrogel sample was placed on the Scanning electron microscope (SEM) section table for gold-spraying treatment. The morphology of the freeze-dried hydrogel sample was examined by SEM.

4.3. Swelling rate testing

The hydrogels were placed in 20 mL Phosphate Buffered Saline (PBS) in a sealed vial at 37 °C. When the preset time interval is reached, remove the hydrogel from the solution and use filter paper to absorb superficial water. After that, weigh the hydrogel. The test is not complete until the weight of all hydrogels remains constant. Each group was measured in parallel 3 times.

Swelling Rate is calculated as follows: Swelling Rate= $(W_t\text{-}W_0)/W_0 \times 100\%$, where W_0 and W_t represent the initial weight of the hydrogel and the weight after the preset expansion time, respectively.

4.4. Water retention testing

The initial weight of the hydrogel (W_0) is accurately weighed and then placed in an incubator at 37 °C for three days, the weight of the sample (W_t) is accurately measured every day, and the water retention rate of the hydrogel is calculated as follows: Water retention rate (%) = $W_t/W_0 \times 100$ %, where W_t and W_0 are the weight of the composite hydrogel on day t and day 0, respectively. Each group was measured in parallel 3 times.

4.5. In vitro degradation testing

The HA-DA@rhCol hydrogel sample was prepared and freeze-dried at −20 °C for 24 h, with initial weight (W_0) accurately weighed. The freeze-dried sample was immersed in PBS (pH 5.5) and PBS solution containing 1 U/mL lysozyme at 37 °C. The hydrogel sample was removed and washed with pure water 3 times at a predetermined time interval, then freeze-dried and weighed (W_t). The degradation rate of hydrogel is calculated as follows: Degradation rate (%) =$(W_0.W_t)/W_0 \times 100\%$, where W_t and W_0 are the weight of the composite hydrogel on day t and day 0, respectively. Each group was measured in parallel 3 times.

4.6. Mechanical properties of hydrogel

Hydrogel samples were prepared into cylindrical shape (~8 mm high × 10.0 mm in diameter) for compression test at 25 °C. The test was investigated using a rheometer (Model DHR-2, TA Instruments) with a speed of 6 mm/min at 60% strain and then recovered to 0% strain with a speed of 6 mm/min. This cycle was repeated for 50 times to determine the compressive and recovery properties. All these tests were employed more than 5 times.

The mechanical tensile stress-strain evaluation was carried out by the uniaxial tensile test employing a materials test system (MTS Criterion 43; MTS Criterion) equipped with a 50 N tension sensor at room temperature. All the hydrogel samples were prepared into stripes (30 mm in length × 6 mm in width × 200 μm in thickness). The tensile strength and elongation at break were obtained at a crosshead rate of 2 mm/min.

4.7. Cytocompatibility evaluation of hydrogels

NIH-3T3 was used for MTT experiment and The Live/Dead staining assay. Hydrogel samples of 1.5% (w/v) HA, 1.5% (w/v) HA-DA, and 1.5% (w/v) HA-DA@rhCol were prepared and incubated in 1 mL of DMEM medium for 24 h to obtain the extraction solution. 0.1 mL (5×10^3 cells/mL) of NIH-3T3 cells were seeded in a 96-well plate, the supernatant was replaced on days 1, 2, and 3, and 10 μL of MTT solution (5 mg/mL) was added to each well. After further incubation for 3 h, the supernatant was discarded, and 200 μL of DMSO was added to each well. Subsequently, 200 μL of the MTT supernatant was transferred to another 96-well plate, and the absorbance at 490 nm (OD) was measured using a multi-functional microplate reader. The cell proliferation rate was calculated as follows: Cell proliferation rate = $(OD_e - OD_b)/(OD_c - OD_b) \times 100\%$ where OD_e represents the experimental group, OD_b represents the blank group, and OD_c represents the control group.

The Live/Dead staining assay was performed to determine cell viability. The wells were washed three times with PBS, and then 100 μL of dye solution containing 1 mM cell viability dye (AM) and 2.5 mg/mL propidium iodide (PI) was added to the wells in the incubator for 30 min. The stained cells were visualized using a confocal laser scanning microscope (CLSM).

4.8. ROS-scavenging testing

RAW264.7 macrophage cell line was used as the experimental cell line. 1 mL of cells (5×10^5 cells/well) were seeded in a 12-well plate and co-cultured with each group of hydrogel samples for 12 h. After that, the cells were washed three times with serum-free medium, and DCFH-DA probe (10 mM, 1 μL) was added to each well. The cells were incubated at 37 °C for 1 h, followed by the addition of H_2O_2 (300 mM, 1 μL) for 20 min. The culture medium was then discarded, and the cells were washed three times with PBS to remove the DCFH-DA probe that did not enter the cells. The cells were observed under a confocal laser scanning microscope (CLSM) as well as detected with Flow Cytometry.

4.9. Photothermal activity testing

Light-thermal performance testing was conducted to evaluate the heat conversion capability of the hydrogels under near-infrared (NIR) laser irradiation. The temperature changes were recorded using an infrared thermal camera. The 1.5% (w/v) HA, 1.5% (w/v) HA-DA, and 1.5% (w/v) HA-DA@rhCol composite hydrogels were placed in tubes. The hydrogels were irradiated with NIR laser (808 nm, 2.0 W/cm^2) for 5 min, and the temperature variations were recorded. Subsequently, the HA-DA@rhCol composite hydrogel was irradiated with NIR (808 nm) at different power densities (0.5, 1.0, and 2.0 W/cm^2) for 5 min, and the temperature changes were recorded. The HA-DA@rhCol composite hydrogel was subjected to four laser on-off cycles using NIR (808 nm, 1.0 W/cm^2). In each cycle, the irradiation time was set to 7.5 min, followed by a cooling period of 7.5 min. The temperature changes were recorded throughout the process.

4.10. The antibacterial performance testing

100 μL of activated *Staphylococcus aureus* (*S. aureus*) and *Escherichia coli* (*E. coli*) with a concentration of 1×10^8 CFU/mL was separately mixed with different hydrogels in a 24-well plate. The groups included Control, 1.5% HA, 1.5% HA-DA, 1.5% HA-DA + NIR,1.5% HA-DA@rhCol, and 1.5% HA-DA@rhCol + NIR. For the near-infrared light groups (1.5% HA-DA + NIR and 1.5% HA-DA@rhCol + NIR), the hydrogels were exposed to 30 min of 808 nm NIR irradiation while maintaining a temperature of 55 °C. Under sterile conditions, 100 μL of the corresponding airborne bacterial suspension was diluted 10^5-fold, and then 100 μL of the diluted bacterial suspension was spread on LB agar culture medium. The plates were co-incubated at 37 °C for 24 h, and the bacterial colony counts on the LB agar plates were observed and counted. In addition, after treatments, bacteria were washed with PBS and fixed with 4% PFA, then were dehydrated by graded ethanol solutions. Finally, the morphologies of dried bacteria were observed by SEM.

4.11. Cell wound scratch assay

The cell scratch assay was performed using human immortalized epidermal cells (HaCaT). 1 mL of HaCaT cells (2.5×10^5 cells/well) was seeded in a 12-well plate and placed in a 37 °C incubator with 5% CO_2 for 12 h. A scratch was made on the cell layer using a pipette tip at a constant speed, ensuring it is perpendicular to the cell plane. The wells were then washed three times with PBS to remove the detached cells. Hydrogel samples of 1.5% (w/v) HA, 1.5% (w/v) HA-DA, and 1.5% (w/v) HA-DA@rhCol were introduced into the respective groups' medium and co-cultured with HaCaT cells. At 0 h and 24 h, the cells were taken out and photographed using a fluorescence inverted microscope to document the migration of cells in each group. The migration rate was calculated as follows: Migration rate (%) = $(R_o - R_s)/R_o \times 100\%$ where R_o is the initial scratch area and R_s is the remaining scratch area after 24 h.

4.12. Tube formation assay

Before tube formation assay, 1.5% HA, 1.5% HA-DA, and 1.5% HA-DA@rhCol were immersed into ECM (Endothelial cell Culture-Medium)

of the corresponding group at 37 °C for 12 h. Then, Matrigel was taken from −20 °C refrigerator and melted in ice for one night, a total of 50 μL of Matrigel was added into each well of a 96-well plate using a pipette and placed into an incubator at 37 °C for 30 min. The new generations of HUVECs were resuspended for 2×10^5 cells/mL by each group of ECM, 100 μL cell suspension were added into Matrigel coated wells, 2×10^4 cells per well, and three wells were set for each group. The plate was cultivated at 37 °C for 12 h, then the tube formation ability of each group was observed and photographed. The experiment was done three times and the number of nodes of tube formation was calculated using a computer software.

4.13. Animal experiments

Animal experiments were conducted in accordance with the Guidelines for National Research Council's Guide for the Care and Use of Laboratory Animals. Male Sprague-Dawley (SD) rats, six weeks old (weighting 200–250 g). Following a four-week period of being fed a high-fat diet, the SD rats were administered a single injection of freshly dissolved streptozotocin (STZ) at a dose of 35 mg/kg in a 0.1 M citrate buffer (pH 4.5) intraperitoneally. After one week, the rats with fasting random blood glucose levels exceeding 16.7 mM were selected as the type II diabetic rats.

After feeding the type II diabetic rats normally for 8 weeks, all diabetic rats were anesthetized by intraperitoneal injection of a 4% (w/w) pentobarbital solution (0.2 mg/100 g). A 10 mm full-thickness excisional wound was created using a 10 mm punch biopsy. The rats were randomly divided into four groups: the blank group (tr), 1.5% HA, 1.5% HA-DA, and 1.5% HA-DA@rhCol groups. Photographic documentation of all wounds was performed at 0, 3, 7, 11, and 15-days post-wounding. The digital images were analyzed using ImageJ software, and the percentage of wound closure was calculated using the following formula: Wound closure rate $= (A_0 - A_t)/A_0 \times 100\%$, where A_0 represents the initial wound area, and A_t represents the wound area at each time point post-wounding.

4.14. Statistical analysis

All statistical analyses were performed via the independent *t*-test between the two groups and one-way ANOVA among multiple groups. At least triplicate experiments were conducted to obtain data, expressed as mean ± SD. A p-value below 0.05 was considered significant and indicated with asterisk: ***P < 0.001, **P < 0.01, *P < 0.05.

Ethics approval and consent to participate

Animal experiments were conducted in accordance with the Guidelines for Animal Care and Use Committee of Zhejiang University.

Declaration of competing interest

The authors declare that they have no known competing financial interests or personal relationships that could have appeared to influence the work reported in this paper.

Data availability statement

The data presented in the study are included in the article, further inquiries can be directed to the corresponding author.

CRediT authorship contribution statement

Yong Wang: Writing – review & editing, Writing – original draft, Methodology, Conceptualization. **Yuan Zhang:** Writing – review & editing, Methodology, Data curation. **Yun-Peng Yang:** Writing – review & editing, Methodology. **Ming-Yuan Jin:** Writing – review & editing, Methodology. **Sha Huang:** Writing – review & editing, Methodology. **Ze-Ming Zhuang:** Writing – review & editing, Methodology. **Tao Zhang:** Writing – review & editing, Methodology. **Li-Li Cao:** Writing – review & editing, Methodology. **Xiao-Ying Lin:** Writing – review & editing, Methodology, Funding acquisition. **Jun Chen:** Project administration, Conceptualization. **Yong-Zhong Du:** Project administration, Conceptualization. **Jian Chen:** Project administration, Conceptualization. **Wei-Qiang Tan:** Writing – review & editing, Project administration, Funding acquisition, Conceptualization.

Acknowledgements

Y.W., Y.Z. and YP.Y. contributed equally to this work. We thank Xiaoli Hong and Chao Bi from the Core Facilities, Zhejiang University School of Medicine for their technical support. This work was supported by grants from National Natural Science Foundation of China No. 82172206, Zhejiang Provincial Medical and Healthy Science Foundation of China (No. 2023RC183 and 2024KY110).

Appendix A. Supplementary data

Supplementary data to this article can be found online at https://doi.org/10.1016/j.bioactmat.2024.02.010.

References

[1] S.M. Aitcheson, F.D. Frentiu, S.E. Hurn, K. Edwards, R.Z. Murray, Skin wound healing: normal macrophage function and macrophage dysfunction in diabetic wounds, Molecules (2021) 26.
[2] M. Rodrigues, N. Kosaric, C.A. Bonham, G.C. Gurtner, Wound healing: a cellular perspective, Physiol. Rev. 99 (2019) 665–706.
[3] J.P. Junker, E.J. Caterson, E. Eriksson, The microenvironment of wound healing, J. Craniofac. Surg. 24 (2013) 12–16.
[4] D.F. Bandyk, The diabetic foot: pathophysiology, evaluation, and treatment, Semin. Vasc. Surg. 31 (2018) 43–48.
[5] R.M. Martínez García, R.M. Fuentes Chacón, A.M. Lorenzo Mora, R.M. Ortega Anta, Nutrition in the prevention and healing of chronic wounds. Importance in improving the diabetic foot, Nutr. Hosp. 38 (2021) 60–63.
[6] M. Zubair, J. Ahmad, Role of growth factors and cytokines in diabetic foot ulcer healing: a detailed review, Rev. Endocr. Metab. Disord. 20 (2019) 207–217.
[7] L.W. Fui, M.P.W. Lok, V. Govindasamy, T.K. Yong, T.K. Lek, A.K. Das, Understanding the multifaceted mechanisms of diabetic wound healing and therapeutic application of stem cells conditioned medium in the healing process, J Tissue Eng Regen Med 13 (2019) 2218–2233.
[8] G. Li, C.N. Ko, D. Li, C. Yang, W. Wang, G.J. Yang, C. Di Primo, V.K.W. Wong, Y. Xiang, L. Lin, D.L. Ma, C.H. Leung, A small molecule HIF-1α stabilizer that accelerates diabetic wound healing, Nat. Commun. 12 (2021) 3363.
[9] Y. Guan, H. Niu, Z. Liu, Y. Dang, J. Shen, M. Zayed, L. Ma, J. Guan, Sustained oxygenation accelerates diabetic wound healing by promoting epithelialization and angiogenesis and decreasing inflammation, Sci. Adv. 7 (2021).
[10] Y. Wang, L. Chen, D.Y. Ren, Z.X. Feng, L.Y. Zhang, Y.F. Zhong, M.Y. Jin, F.W. Xu, C.Y. Feng, Y.Z. Du, W.Q. Tan, Mussel-inspired collagen-hyaluronic acid composite scaffold with excellent antioxidant properties and sustained release of a growth factor for enhancing diabetic wound healing, Mater Today Bio 15 (2022) 100320.
[11] H. Cortes, I.H. Caballero-Florán, N. Mendoza-Muñoz, E.N. Córdova-Villanueva, L. Escutia-Guadarrama, G. Figueroa-González, O.D. Reyes-Hernández, M. González-Del Carmen, M. Varela-Cardoso, J.J. Magaña, B. Florán, M.L. Del Prado-Audelo, G. Leyva-Gómez, Hyaluronic acid in wound dressings, Cell. Mol. Biol. 66 (2020) 191–198.
[12] I.S. Bayer, Hyaluronic acid and controlled release: a review, Molecules (2020) 25.
[13] B.A. Mast, L.C. Flood, J.H. Haynes, R.L. DePalma, I.K. Cohen, R.F. Diegelmann, T. M. Krummel, Hyaluronic acid is a major component of the matrix of fetal rabbit skin and wounds: implications for healing by regeneration, Matrix 11 (1991) 63–68.
[14] D.H. Lee, J.H. Oh, J.H. Chung, Glycosaminoglycan and proteoglycan in skin aging, J. Dermatol. Sci. 83 (2016) 174–181.
[15] W.S. Parkes, F. Amargant, L.T. Zhou, C.E. Villanueva, F.E. Duncan, M.T. Pritchard, Hyaluronan and collagen are prominent extracellular matrix components in bovine and porcine ovaries, Genes (2021) 12.
[16] E. Davison-Kotler, W.S. Marshall, E. García-Gareta, Sources of collagen for biomaterials in skin wound healing, Bioengineering (Basel) (2019) 6.
[17] W. Liu, H. Lin, P. Zhao, L. Xing, J. Li, Z. Wang, S. Ju, X. Shi, Y. Liu, G. Deng, G. Gao, L. Sun, X. Zhang, A regulatory perspective on recombinant collagen-based medical devices, Bioact. Mater. 12 (2022) 198–202.
[18] A. Sorushanova, L.M. Delgado, Z. Wu, N. Shologu, A. Kshirsagar, R. Raghunath, A. M. Mullen, Y. Bayon, A. Pandit, M. Raghunath, D.I. Zeugolis, The collagen suprafamily: from biosynthesis to advanced biomaterial development, Adv Mater 31 (2019) e1801651.

[19] Y. Wang, J.Y. Ji, K. Guo, T. Zhang, X.C. Zhong, Z.M. Zhuang, Y.F. Zhong, X.Y. Lin, Y.Z. Du, J. Chen, W.Q. Tan, Gene liposome nanocomplex-loaded dermal substitute promotes diabetic chronic wound healing and angiogenesis in rat, Biomed. Pharmacother. 163 (2023) 114794.
[20] P. Tang, L. Han, P. Li, Z. Jia, K. Wang, H. Zhang, H. Tan, T. Guo, X. Lu, Mussel-inspired electroactive and antioxidative scaffolds with incorporation of polydopamine-reduced graphene oxide for enhancing skin wound healing, ACS Appl. Mater. Interfaces 11 (2019) 7703–7714.
[21] L. Han, P. Li, P. Tang, X. Wang, T. Zhou, K. Wang, F. Ren, T. Guo, X. Lu, Mussel-inspired cryogels for promoting wound regeneration through photobiostimulation, modulating inflammatory responses and suppressing bacterial invasion, Nanoscale 11 (2019) 15846–15861.
[22] F. Pallaske, A. Pallaske, K. Herklotz, J. Boese-Landgraf, The significance of collagen dressings in wound management: a review, J. Wound Care 27 (2018) 692–702.
[23] K. Ousey, K.F. Cutting, A.A. Rogers, M.G. Rippon, The importance of hydration in wound healing: reinvigorating the clinical perspective, J. Wound Care 25 (122) (2016) 124–130.
[24] H. Cheng, Z. Shi, K. Yue, X. Huang, Y. Xu, C. Gao, Z. Yao, Y.S. Zhang, J. Wang, Sprayable hydrogel dressing accelerates wound healing with combined reactive oxygen species-scavenging and antibacterial abilities, Acta Biomater. 124 (2021) 219–232.
[25] A. Francesko, P. Petkova, T. Tzanov, Hydrogel dressings for advanced wound management, Curr. Med. Chem. 25 (2018) 5782–5797.
[26] X. Wang, R. Song, M. Johnson, S. A, Z. He, C. Milne, X. Wang, I. Lara-Sáez, Q. Xu, W. Wang, An injectable chitosan-based self-healable hydrogel system as an antibacterial wound dressing, Materials 14 (2021).
[27] L. Han, Y. Zhang, X. Lu, K. Wang, Z. Wang, H. Zhang, Polydopamine nanoparticles modulating stimuli-responsive PNIPAM hydrogels with cell/tissue adhesiveness, ACS Appl. Mater. Interfaces 8 (2016) 29088–29100.
[28] Y. Li, R. Fu, C. Zhu, D. Fan, An antibacterial bilayer hydrogel modified by tannic acid with oxidation resistance and adhesiveness to accelerate wound repair, Colloids Surf. B Biointerfaces 205 (2021) 111869.
[29] H. Zhao, J. Huang, Y. Li, X. Lv, H. Zhou, H. Wang, Y. Xu, C. Wang, J. Wang, Z. Liu, ROS-scavenging hydrogel to promote healing of bacteria infected diabetic wounds, Biomaterials 258 (2020) 120286.
[30] Y. Xiong, L. Chen, P. Liu, T. Yu, C. Lin, C. Yan, Y. Hu, W. Zhou, Y. Sun, A.C. Panayi, F. Cao, H. Xue, L. Hu, Z. Lin, X. Xie, X. Xiao, Q. Feng, B. Mi, G. Liu, All-in-One: multifunctional hydrogel accelerates oxidative diabetic wound healing through timed-release of exosome and fibroblast growth factor, Small 18 (2022) e2104229.
[31] Q. Bai, K. Han, K. Dong, C. Zheng, Y. Zhang, Q. Long, T. Lu, Potential applications of nanomaterials and technology for diabetic wound healing, Int. J. Nanomed. 15 (2020) 9717–9743.
[32] Y.H. Lee, Y.L. Hong, T.L. Wu, Novel silver and nanoparticle-encapsulated growth factor co-loaded chitosan composite hydrogel with sustained antimicrobility and promoted biological properties for diabetic wound healing, Mater. Sci. Eng., C 118 (2021) 111385.
[33] K. Gwon, I. Han, S. Lee, Y. Kim, D.N. Lee, Novel metal-organic framework-based photocrosslinked hydrogel system for efficient antibacterial applications, ACS Appl. Mater. Interfaces 12 (2020) 20234–20242.
[34] C. Liu, Z. Shi, H. Sun, L. Zhao, X. Wang, F. Huang, Tissue factor-loaded collagen/alginate hydrogel beads as a hemostatic agent, J. Biomed. Mater. Res. B Appl. Biomater. 109 (2021) 1116–1123.
[35] Q. Xu, J.E. Torres, M. Hakim, P.M. Babiak, P. Pal, C.M. Battistoni, M. Nguyen, A. Panitch, L. Solorio, J.C. Liu, Collagen- and hyaluronic acid-based hydrogels and their biomedical applications, Mater. Sci. Eng. R Rep. 146 (2021).